

Investigation of Flow Field in a Typical Hypersonic Wind Tunnel over a Standard Mode

F. Mohammadifard¹, M. Karami² and M. Heidari^{3†}

^{1,2} Qadr Aerodynamic Research Center, Tehran, Iran

³ Islamic Azad University, Parand Branch, Tehran, Iran

†Corresponding Author Email: mrezaheidari@yahoo.com

(Received April 13, 2012; accepted November 15, 2012)

ABSTRACT

In order to start designing a new hypersonic wind tunnel, it is important to have a pre-view about physical phenomena in a typical Hypersonic Wind Tunnel (HWT). In present research, it is tried to view phenomenologically the aerodynamics of flow in a typical HWT by Computational Fluid Dynamics (CFD). The considered HWT consists of a curved nozzle in nominal Mach number 12, free-jet type test section, a test model and a convergent-divergent diffuser. Aerodynamics of flow in the nozzle exit and test section, conical shock wave system in the diffuser and flow over a standard model (HB-2) are investigated. A method is introduced for numerical simulation of capturing the free shear layer in free-jet test section based on the vorticity distribution of flow. The aerodynamics behavior of HB-2 model is investigated in various Mach numbers and flow domains. The results make a better view of some aerodynamic phenomena in a free-jet type test section of wind tunnel that are rarely considered. This research is conducted towards the project of designing and manufacturing the industrial hypersonic wind tunnel for Qadr Aerodynamic research Center.

Keywords: Hypersonic, Wind tunnel, Standard model, CFD.

NOMENCLATURE

| | | | |
|---------------|---|------------|---------------------------|
| E | internal energy | μ | dynamic viscosity |
| F | force | v | velocity |
| h | enthalpy per mass | ρ | density |
| k | kinetic energy | τ | stress tensor |
| L | model length | ω | turbulence eddy frequency |
| M | Mach number | | |
| P | static pressure | Subscripts | |
| q | dynamic pressure | b | model base |
| R | universal gas constant | r | radial coordinate |
| Re | Reynolds number | T | turbulent |
| S_m | source term of mass | x | axial coordinate |
| T | static temperature | O_s | total stagnation |
| δ | Kronecker's delta function | ∞ | free stream |
| ε | dissipation rate of turbulence kinetic energy | | |

1. INTRODUCTION

Establishment of supersonic and hypersonic flow in the wind tunnels needs very high energy and as test time and flow velocity increase, the needed energy increases with more intensity. For short-time tests in hypersonic flow regimes, usually, shock tubes or piston shock tunnels are used in various run durations. For long duration tests that enable us to have more precise data or having data in unsteady flow, hypersonic wind tunnels are employed. In this case, to prevent

condensation of water vapor in air over model in test section that may cause errors in data from sensors, supplying air must be pre-heated to high temperature values. Because of pre-heating process, the operating air has high enthalpy and so the wind tunnel is called high enthalpy wind tunnel. Considering very high energy needed to setup high Mach numbers by preheating and compressing the supplying air and the huge amount of prices for constructing a new hypersonic wind tunnel for long duration tests, it is important to have a pre-view of aerodynamic

phenomena over model and through components of a hypersonic wind tunnel to reduce mistakes in design procedure. A few developed countries are experienced in hypersonic wind tunnel designing, manufacturing and testing and they can use previous experiences and practical data to design and to construct new wind tunnels. In contrast, there are many countries deprived to have practical data. Thus numerical simulation for these countries can come in handy without spending a lot of money and time. The present research is towards the project of industrial hypersonic wind tunnel designing and manufacturing for Qadr Aerodynamic Research Center that would be the first HWT of Iran. A typical high enthalpy hypersonic wind tunnel includes three main aerodynamics components: Nozzle, test section and diffuser. In most of the cases for hypersonic wind tunnels, the test section is free jet type. Free jet type test section enables operator to have a good access inside the test section and to decrease the chance of test section blockage due to shock wave passing over model at the tunnel start. There are few available researches and numerical simulations about whole hypersonic wind tunnel (nozzle, test section and diffuser). A research conducted by [Chen \(2004\)](#) is addressing the steady and unsteady flow simulations of Virginia Tech hypersonic wind tunnel which has the free jet type test section but it does not include model through test section. In mentioned study, the simulations have been done for inviscid steady and transient flows. Standard models play an important role in wind tunnels calibration. There are many practical data available for them. These data can be used by researchers for validating the simulation data. In the present research, after investigation of some general standard models in high speed flow, including CANs, Cone, re-entry capsules and HB-2, HB-2 model, discussed later, is chosen to be simulated in several conditions including various simulation domains, Mach numbers and pressures. Behavior of standard model HB-2 is investigated by numerical simulations through the test section of a typical HWT and in three different flow conditions through C domain. In the C-domain simulations, the model is located in a C-shaped domain with uniform flow over it. In C-domain cases, the behavior of model in ideal uniform flow can be investigated in addition to simulate the test section of a typical HWT. The results of simulation for HWT show some aerodynamic phenomena in the components of wind tunnel and over model. In all simulations, the angle of attack of the model is zero. There are many experimental researches and investigations available about HB-2 model. A group of researchers from JAXA (2005) made two practical tests in 1.27 Mach wind tunnel and high enthalpy shock tunnel. These researches included force and heat transfer tests but there are no numerical simulation data. Gray and Lindsay (1964) conducted a study on HB-1 and HB-2 models, where the force aerodynamic characteristics of HB-1 and HB-2 were investigated in the supersonic and hypersonic regimes. The tests were conducted at nominal Mach numbers of 1.5, 2, 3, 4, 5, 8, and 10 at Reynolds numbers from 0.07 to 2.55×10^6 based on body diameter and in angles of attack range from -2 to 15 degrees. [Deem \(1961\)](#) made a research to define force and heat characteristics of HB-2 model in Mach numbers from 2 to 5 that includes the effects of shock impingement. All the above mentioned studies and

researches made good data for comparison between experimental and numerical simulation results and on the other hand, they give strong vision of aerodynamic characteristics over HB-2 model.

2. GOVERNING EQUATIONS

The present numerical approach has been engaged for solving the problem under some assumptions such as steady state, axisymmetric flow, compressible perfect gas, turbulent and non-reacting flow. The governing equations can be considered as the mass conservation (or continuity equation), the momentum conservation equations, the energy balance equation and finally, the state equation. The continuity equation can be written as [Eq. \(1\)](#),

$$\frac{\partial \bar{\rho}}{\partial t} + \nabla \cdot (\bar{\rho} \bar{v}) = S_m \quad (1)$$

Where \bar{v} , $\bar{\rho}$ and S_m are density, velocity vector and the mass added to the continuous phase from the dispersed second phase (e.g., due to vaporization of liquid droplets) and any user-defined sources, respectively. Also, the accent bar ($\bar{\cdot}$) represents the long-time-averaged value of instantaneous parameter (\cdot), according to turbulent fluctuations. For 2D axisymmetric geometries, the continuity equation can be written as [Eq. \(2\)](#),

$$\frac{\partial \bar{\rho}}{\partial t} + \frac{\partial}{\partial x} (\bar{\rho} v_x) + \frac{\partial}{\partial r} (\bar{\rho} v_r) + \frac{\bar{\rho} v_r}{r} = 0 \quad (2)$$

where x is the axial co-ordinate, r is the radial co-ordinate, v_x is the axial velocity, and v_r is the radial velocity. The momentum equation, based on Newton's second law, relates the fluid particle acceleration $D\bar{v}/Dt$ to the surface and body forces experienced by the fluid. In general, the surface forces, which are of molecular origin, are described by the stress tensor τ_{ij} which is symmetric, i.e. $\tau_{ij} = \tau_{ji}$. The body force of interest is gravity which can be neglected in the present investigation. Hence, the momentum equation in the general form can be written as [Eq. \(3\)](#).

$$\frac{D(\bar{\rho} \bar{v})}{Dt} = \frac{\partial \tau_{ij}}{\partial x_i} \quad (3)$$

where

$$\tau_{ij} = -P \delta_{ij} + \mu \left(\frac{\partial v_i}{\partial x_j} + \frac{\partial v_j}{\partial x_i} \right) \quad (4)$$

For a 2D axisymmetric flow, the axial and radial momentum conservation equations can be written as [Eq. \(5\)](#) and [Eq. \(6\)](#), respectively:

$$\begin{aligned} & \frac{\partial}{\partial t}(\overline{\rho v_x}) + \frac{1}{r} \frac{\partial}{\partial x}(r \overline{\rho v_x v_x}) + \\ & \frac{1}{r} \frac{\partial}{\partial r}(r \overline{\rho v_r v_x}) = -\frac{\partial p}{\partial x} + \\ & \frac{1}{r} \frac{\partial}{\partial x} \left[r \mu_{eff} \left(2 \frac{\partial \overline{v_x}}{\partial x} - \frac{2}{3} \nabla \vec{v} \right) \right] + \\ & \frac{1}{r} \frac{\partial}{\partial r} \left[r \mu_{eff} \left(\frac{\partial \overline{v_x}}{\partial r} + \frac{\partial \overline{v_r}}{\partial x} \right) \right] \end{aligned} \quad (5)$$

$$\begin{aligned} & \frac{\partial}{\partial t}(\overline{\rho v_r}) + \frac{1}{r} \frac{\partial}{\partial x}(r \overline{\rho v_x v_r}) + \\ & \frac{1}{r} \frac{\partial}{\partial r}(r \overline{\rho v_r v_r}) = -\frac{\partial p}{\partial x} + \\ & \frac{1}{r} \frac{\partial}{\partial x} \left[r \mu_{eff} \left(\frac{\partial \overline{v_x}}{\partial r} + \frac{\partial \overline{v_r}}{\partial x} \right) \right] \\ & + \frac{1}{r} \frac{\partial}{\partial r} \left[r \mu_{eff} \left(2 \frac{\partial \overline{v_r}}{\partial r} - \frac{2}{3} \nabla \vec{v} \right) \right] \\ & - 2 \mu \frac{v_r}{r^2} + \frac{2}{3} \frac{\mu_{eff}}{r} (\nabla \vec{v}) + \rho \frac{v_x}{r} \end{aligned} \quad (6)$$

where

$$\nabla \vec{v} = \frac{\partial v_x}{\partial x} + \frac{\partial v_r}{\partial r} + \frac{v_r}{r} \quad (7)$$

It is noticeable that μ_{eff} represents total dynamic viscosity. In general form, the energy conservation concept can be formulated as Eq. (8).

$$\begin{aligned} & \frac{\partial}{\partial t}(\rho E) + \nabla \cdot [\vec{v}(\rho E + p)] = \\ & \nabla \cdot [k_{eff} \nabla T + \tau_{ij} \vec{v}] \end{aligned} \quad (8)$$

where

$$E = h - \frac{p}{\rho} + \frac{v^2}{2} \quad (9)$$

For compressible flows, the equation of state (considering ideal-gas concept) can be written as Eq. (10).

$$\frac{p}{\rho} = RT \quad (10)$$

In which, R is the universal gas constant. According to the Boussinesq approximation, the Reynolds stresses can be related to the local velocity gradients by defining the turbulent eddy viscosity as in Eq. (11).

$$\overline{\rho u_i' u_j'} = \mu_t \frac{\partial u_i}{\partial x_j} \quad (11)$$

A pair of turbulence scalar quantities, such as $k - \varepsilon$ or $k - \omega$ may be used to calculate the turbulent eddy

viscosity. In the present study, the Shear Stress Transport (SST) model has been chosen for solving the turbulence characteristics of flow. The SST/ $k - \omega$ turbulence model is a two-equation eddy-viscosity model. The use of a formulation in the inner parts of the boundary layer makes the model directly usable close to the wall through the viscous sub-layer. Hence, the SST/ $k - \omega$ may be used as a low-Re turbulence model without any additional damping function. The SST formulation also switches to a $k - \varepsilon$ behavior at fully turbulent flow fields and hence it avoids the common $k - \omega$ problem where the model is too sensitive to the inlet free stream turbulence properties. The turbulence kinetic energy, k and the specific dissipation rate, ω are represented by Eq. (12) and Eq. (13), respectively. In these equations, β and σ are closure coefficients and F and S are auxiliary relations.

$$\begin{aligned} & \frac{\partial k}{\partial t} + u_j \frac{\partial k}{\partial x_j} = P_k - \beta^* k \omega + \\ & \frac{\partial}{\partial x_i} \left[(v + \sigma_k v_T) \frac{\partial k}{\partial x_i} \right] \end{aligned} \quad (12)$$

$$\begin{aligned} & \frac{\partial \omega}{\partial t} + u_j \frac{\partial \omega}{\partial x_j} = \alpha S^2 - \beta \omega^2 + \\ & \frac{\partial}{\partial x_i} \left[(v + \sigma_\omega v_T) \frac{\partial \omega}{\partial x_i} \right] + \\ & 2(1 - F_1) \sigma_{\omega 2} \frac{1}{\omega} \frac{\partial k}{\partial x_j} \frac{\partial \omega}{\partial x_j} \end{aligned} \quad (13)$$

Thus, μ_t can be obtained from Eq. (14).

$$\mu_t = \frac{a_1 k}{\max(a_1 \omega, S F_2)} \quad (14)$$

3. MODEL GEOMETRY AND GRID GENERATION

There are two types of domain considered for simulations. The first domain is C-shaped domain which consists of a bow and a vertical line. The second domain is the preliminary designed hypersonic wind tunnel which consists of a curved nozzle from the throat that creates a uniform flow at Mach 12, a free jet type test section and a diffuser with convergent, throat and divergent parts. Figure 2 shows a HB-2 model in test section of the wind tunnel; No. 1, 3 and 4 are nozzle, test section and diffuser entrance, respectively. In the ideal case, the uniform flow exists in the some parts of nozzle exit and can be used as a test area, but in this case, the model is installed just after the nozzle exit. This wind tunnel is designed for special purposes for Iranian aerospace needs. The C-domain is used to simulate Mach numbers 5, 9.59 and 12. The solution domain for C-type domain is shown in Fig. 3. Figure 4 shows the boundary layer meshing around the model. The mostly tracked property is the distribution of static pressure over the model. It is important to make grids in the way that shock wave and grid surfaces to be parallel, especially for the nose domain, otherwise

capturing the shock wave will not be precise. For this reason, structured mesh employed near body that covers both the normal part of bow shock wave and boundary layer.

4. STANDARD MODELS FOR HYPERSONIC TESTS

There are many models employed for high-speed wind tunnel testing. For present research, CANs, Cone types, Re-entry capsules and HB1&2 models are nominated for investigation. The purpose of this consideration is to define the best model for hypersonic Mach numbers. The CANs are the axisymmetric models with a sharp nose and sharp flare that are not proper for hypersonic tests. It is obvious that in hypersonic flow, the nose must be blunted to avoid melting by very high temperature which occurs after the normal shock wave in front of nose. The cone-shaped models have sharp nose, so they are not proper for hypersonic tests too. Re-entry capsule models have blunted nose, but they are short in length and their body shapes are very simple, so some aerodynamic phenomena such as boundary layer weakness, contractions and expansion waves do not happen over model. The HB-2 model is relatively simple; therefore, it reduces uncertainties coming from the geometry complexity for data comparison. This model has an analytical shape that consists of a sphere at nose, cylinder at body and flare at base, so mentioned phenomena can be detected over it, also the HB-2 model is totally axisymmetric. The geometry of a typical HB-2 model is shown in Fig. 1. It is not too short and it is expected that a bow shock being formed just in front of the model. The employed HB-2 model is a standard model proposed by AGARD. For present study, the material of model is steel with fine polished surface. However, the heat transfer is not considered in the body of model, but the roughness of the body has a significant role in the formation and physics of boundary layer.

5. METHODOLOGY OF NUMERICAL SIMULATIONS

The congestion of grid in boundary layer is enough for obtaining results with the least errors. The total numbers of cells are 252000 for C-domain. The grid-independency study had been conducted by the authors of present research in previous investigation by Ameri *et al.* (2011). The boundary condition for free stream, defines the Mach number, static temperature and static pressure of free stream. The flow considered as an ideal gas with the various C_p as a function of temperature; in this case two polynomial models with eight coefficients in two range of temperature are employed. The viscosity is considered as a function of temperature and the Sutherland's model with three coefficients is used. The boundary condition over model is wall with no slip and heat transfer. For simulating the viscosity, shear stress transport model (SST) with transient effect and laminar model for HWT simulations and laminar flow for Case-1, 2 and 3 were chosen. In the other research conducted by the authors of present research [9], it is shown that SST makes reasonable results for turbulent hypersonic flow simulations in HWT.

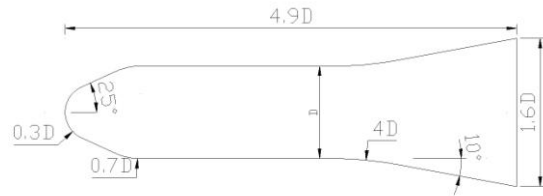


Fig. 1. Typical HB-2 model geometry, D is main body diameter.

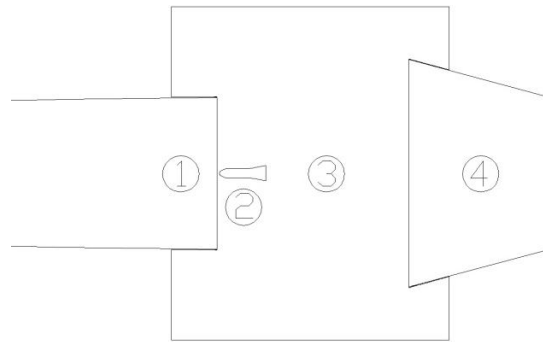


Fig. 2. HB-2 model location in test section.

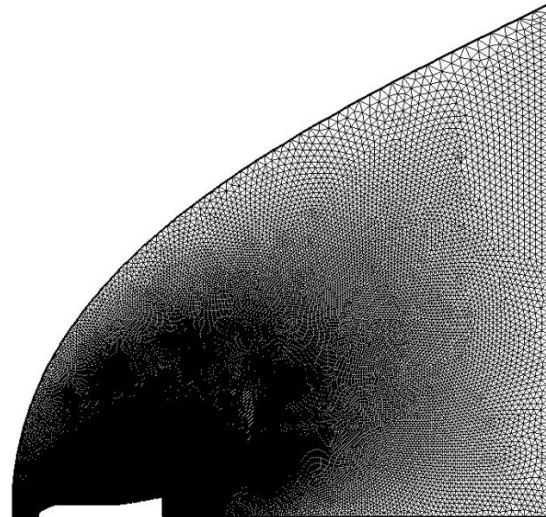


Fig. 3. Grid over C-Domain.

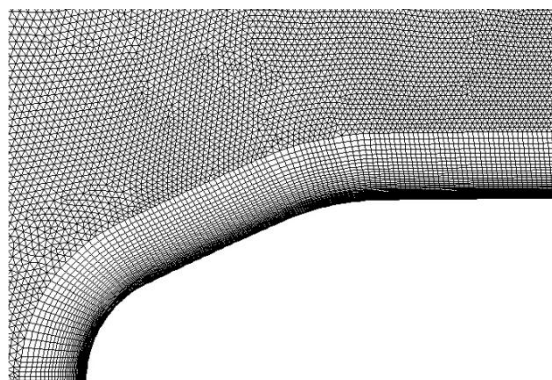


Fig. 4. Grid over nose of HB-2.

The computational domain consists of nozzle throat, test section and diffuser and it has 440000 computational cells. In all components of flow domain there is boundary layer mesh with congestion near walls. The boundary condition in the throat of nozzle is set as the ratio of static pressure to the total pressure of 0.528 in order to generate Mach number of one. All walls including walls of model are adiabatic with no slip condition. As same as C-domain simulations, the Cp and viscosity are considered as the functions of temperature. For simulating turbulence behavior of flow, the SST/k- ω model is engaged. Values for aerothermodynamics parameters assigned for numerical simulations for HWT and C-domain are shown in Table 1. Reynolds numbers are based on center body diameter. All simulations are done for steady-state and axisymmetric flow domain and model is installed in the zero angle of attack, so only half of model and flow domain are needed for simulations. As it is shown in Table 1, Reynolds numbers are low in all cases, so it is logical to assume that the flow field is laminar in solution domain, nevertheless, for HWT case, simulations are done for both laminar and turbulent flows in transient form.

Table 1. Flow properties for simulations.

| Parameter | Case-1 | Case-2 | Case-3 | HWT |
|---------------------------|--------|--------|--------|-------|
| M | 5 | 9.59 | 12 | 12 |
| T (K) | 99.55 | 75 | 67.75 | 67.75 |
| P (Pa) | 1142 | 52 | 81.89 | 81.89 |
| Re $\times 10^6$ (1/m) | 0.48 | 2.06 | 0.02 | 0.02 |
| Model Length (cm) | 49 | 49 | 18.38 | 18.38 |

6. RESULTS AND DISCUSSION

The research conducted by Gray and Lindsay (1964) has variety in Mach numbers over HB-2 model. The simulation of HB-2 for Case-1 is based on mentioned research in Mach number 5. Distribution of the static pressure over HB-2 model by simulation and practical data shows a good compatibility. This is shown in Fig. 5. There are two pressure drops before $x/L=0.2$ which are related to the two expanding curves in the fore-body of model. There is a slight rise on pressure just after $x/L=0.6$ which is related to the contraction waves in the joint of body and flare. In the practical data analysis, it is shown that just before $x/L=0.6$ there is a small flow separation. Figure 6 shows velocity vectors just before $x/L=0.6$ in flow separation zone. The flow separation occurred because of weak laminar boundary layer and compressive shock wave.

The simulation for Case-2 is based on researches conducted in JAXA introducing the fore-body axial force coefficient in the zero angle of attack, C_{AF0} . Practical data from wind tunnel and calculations show

the value of $0.59 \pm 3\%$ for C_{AF0} . For Case-2, this value is 0.6 which has a good compatibility to practical value.

$$C_{AF0} = \frac{F_x - [(P_\infty - P_b) \times A_b]}{q_\infty \times A} \quad (15)$$

Case-3 is determined to have a comparison data between wind tunnel and C-domain simulation results. For this case, Mach number, static pressure and other aerothermodynamics parameters are considered to be same as HWT nozzle exit flow conditions.

It is important to have a uniform flow at the exit of the nozzle to have an appropriate test. In this case, chosen curved nozzle provides a very good uniform velocity flow just in the nozzle exit. The distribution of velocity magnitude in the nozzle exit is shown in Fig. 7 where the boundary layer thickness is about 33% of nozzle exit diameter. The aspect ratio of model to nozzle exit area in HWT is 1% to prevent tunnel to choke.

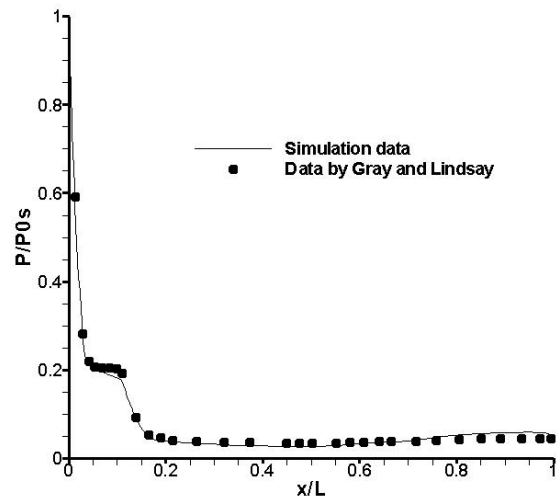


Fig. 5. Distribution of static pressure over model for Case-1.

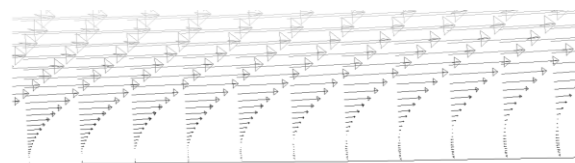


Fig. 6. Velocity vectors show flow separation just before $x/L=0.6$ for Case-1.

In the free jet type test section, there are two separated flow domains. The first is located where the core flow exists and the second is dead flow around the core flow, which is called dead flow chamber. The definition of boundary which separates core and dead flows is important to find the proper space to measure the thickness of the model and to design the diffuser jet catcher. According to simulation data and the physics of flow, the boundary between the flow jet and the dead flow in both sides has the same static pressure and velocity vector but the entropy is different. These characteristics belong to a phenomenon called free flow shear layer known as sleep line. In the shear layer, high vorticity flow exists. This is because of differences in velocity magnitude. This make us to recognize the exact

position of free flow shear layer along the axis of test section. For this reason, five cross-sectional stations with equal distances from nozzle exit to diffuser inlet are determined along the axis of test section and the magnitude of vorticity were extracted. Figure 8 shows the results. The height of peak for each station before the radius of 0.3 meters allocates to the position of shear layer or Slip Line. As flow goes through test section, the vorticity magnitude is weakening. High vorticity peaks near radius zero belong to model wall. Contours of the stream function in the test section are shown in Fig. 9. The vortexes in dead flow chamber are visible and this part of flow doesn't have a direct role in core flow quality. Jet catcher is the first part of the diffuser that captures the core flow. At this place, conical shock wave system begins to decelerate the flow. A portion of shock wave systems from the jet catcher to the end of throat of diffuser is shown in Fig. 10. For simulated wind tunnel, jet-catcher captures whole core flow and sends it to the diffuser.

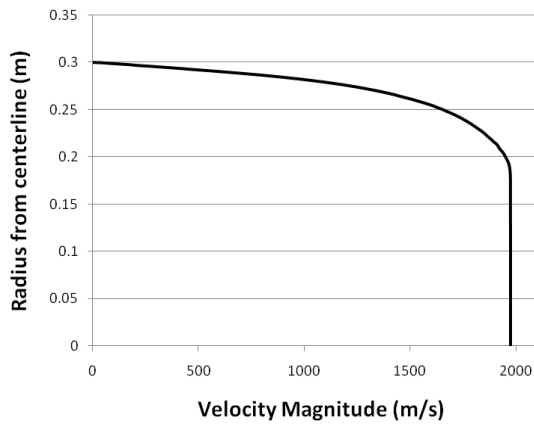


Fig. 7. Distribution velocity magnitude in the exit of the nozzle of HWT.

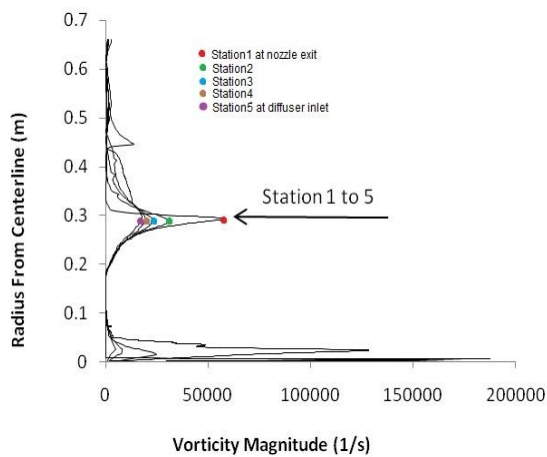


Fig. 8. Distribution of vorticity for 5 cross sectional station in test section.

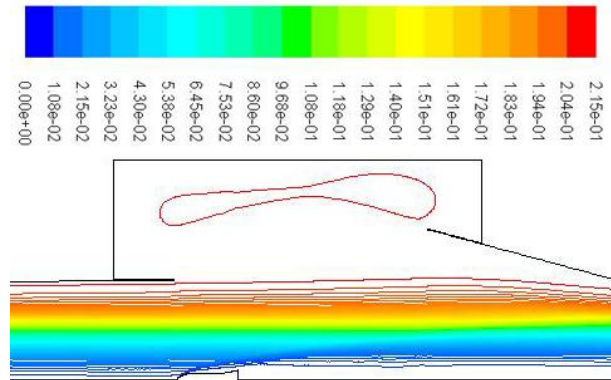


Fig. 9. Contours of stream function (kg/s) through test section of HWT

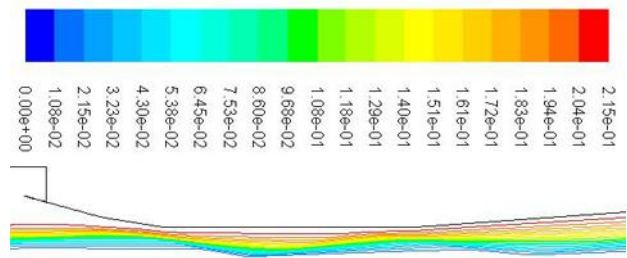


Fig. 10. Contours of stream function (kg/s) through diffuser of HWT.

In order to find the behavior of boundary layer, distribution of skin friction coefficient over the model is investigated. Figure 11 shows the values of skin friction over model for Case-1, 2, 3 and HWT. There are two peaks between $x/L=0$ and $x/L=0.2$ related to two expansions in the nose of model which increase the skin friction coefficient. There are falls for Case-2 and 3 and HWT, between $x=0.6$ to 0.8 . These minimums show weakened boundary layer places due positive static pressure gradient just in the joint of body and flare. Among the cases, Case-1 has two minimum values. The first minimum shows flow separation just before $x/L=0.6$ and the second one just before $x/L=0.8$ shows re-attached flow. Skin friction coefficient for HWT has maximum value because of turbulent flow assumption.

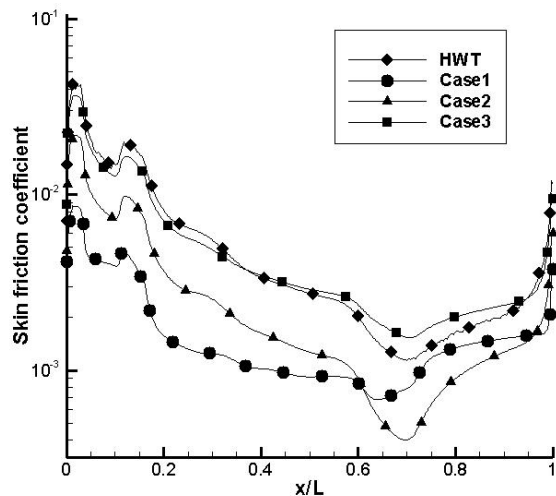


Fig. 11. Distribution of skin friction coefficient over model for all simulation cases.

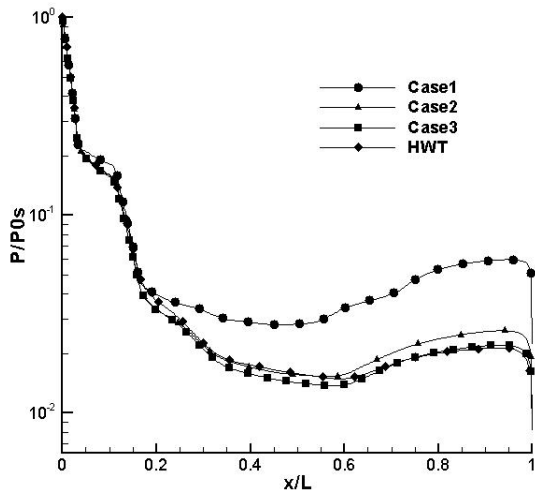


Fig. 12. Distribution of static pressure over model for all simulation cases.

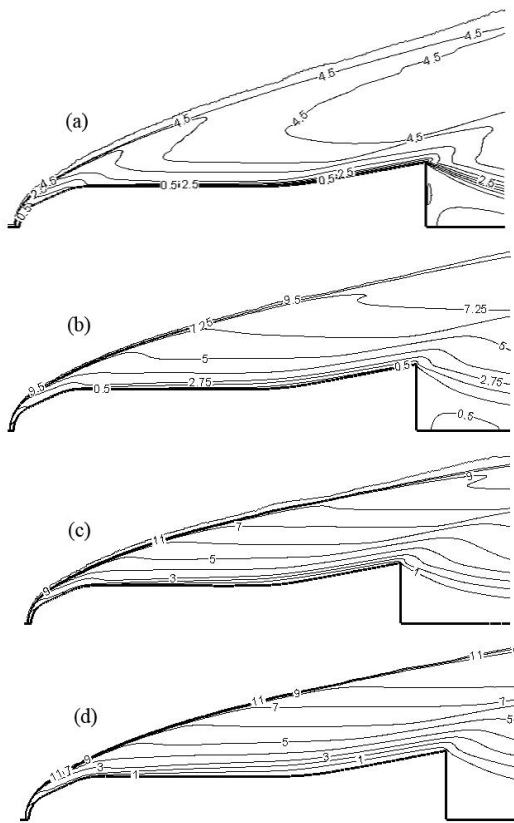


Fig. 13. Contours of Mach number over model a) Case-1, b) Case-2, c) Case-3, and d) HWT.

In order to make comparison between all simulations, static pressure distributions for all cases are shown in Fig. 12. Because of low Case-1 has the maximum static pressure and other cases stay almost in the same range. The rates of increase in static pressure in $x/L=0.6$ are almost the same.

Figure 13 shows the contours of Mach number over model in all cases. As the free stream Mach number increases, the flare of bow shock bends toward the model body that is predictable. In all cases, at the base of model there is a vortex that makes a pressure drag.

This vortex is shown in Fig. 14 for HB-2 in HWT domain.

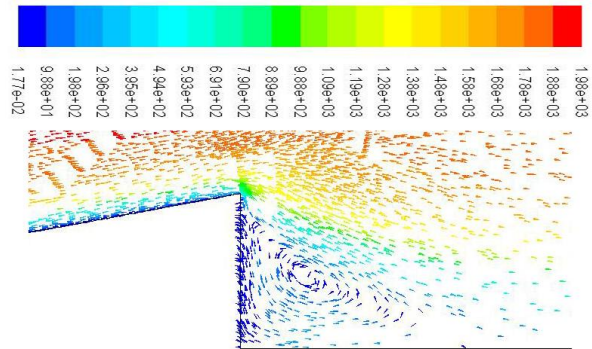


Fig. 14. Vectors of velocity magnitude in the model base.

7. CONCLUSIONS

By comparing results of numerical simulations for Case-1 and Case-2 with practical data including static pressure distribution over model, it is shown that in the high velocity force simulations in the supersonic and hypersonic regimes, the results are reliable. By comparing the results of Case-3 and practical data from wind tunnel, it is shown that there is a good compatibility for force simulations between external flow data for C-domain from simulations and internal flow data from HWT over model, also simulations data of Case-3 and HWT show very good compatibility. It means that the simulations for external and internal flows for a sample Mach number have very close results. It is shown that for studied typical HWT, the ratio 1% of cross-section area of the thickest section of model to the nozzle exit area is enough to avoid tunnel choking in steady run. A method is introduced to determine the exact location of free flow shear layer by considering the vorticity of flow. It helps to design a better jet catcher for diffuser that is very important to reduce the energy needed for run of a hypersonic wind tunnel. The behavior of boundary layer over model is investigated for four cases by considering the skin friction coefficient, and the behavior of the flow around HB-2 model is determined. The results come in handy for designing a new hypersonic wind tunnel, also for predicting the behavior of flow over HB-2 model which is chosen as a very good standard model for predicting the components behavior of a typical hypersonic wind tunnel. Future works are considered to be transient and non-adiabatic flow simulations for simulating force and thermal effects also by considering non-zero angle of attack for 3D models.

REFERENCES

- Ameri, M.J., E. Karami (2011). Assessment of turbulence models for investigating of hypersonic flow through an industrial wind tunnel. *Proceedings of the 10th Conference of Iranian Aerospace Society, Tarbiar modarres university Tehran, Iran, March*. 183-184.

- Baldwin, L. (1955). Viscous effects on static pressure distribution for a slender cone at a nominal Mach number of 5.8. BSc. *Dissertation, California institute of technology, California.*
- Burcham, F.W. (1968). Wind-Tunnel calibration of a 40° conical pressure probe at Mach numbers from 3.5 to 7.4. *NASA TN D-4678.*
- Chen, R. (2004). Computational studies of the Virginia Tech hypersonic wind tunnel. *Proceedings of the Virginia Tech Symposium for undergraduate research in engineering, Virginia Polytechnic Institute and State University, USA, Oct.*
- Deem, R.E. (1961). Pressure and heat-transfer distribution tests on a standard ballistic-type model HB-2 at mach 2 to 5, including the effects of shock impingement. *Report S-R6, Douglas Aircraft Company, California, USA, Jun.*
- Dupuis, A.D., and J.A., Edwards (1995). Flight tests and computational analysis of two hypersonic research projectiles. *Proceedings of the 33rd Aerospace sciences meeting and exhibit, Reno, NV.*
- Gray, J.D. and E.E. Lindsay (1964). Summary report on aerodynamic characteristics of standard model HB-1 and HB-2. *Technical report AEDC-TDR-63-137, Arnold engineering development center, USA.*
- Kuchi-Ishi, Sh. and E. Watanabe (2005). Comparative force/heat flux measurements between JAXA hypersonic test facilities using standard model HB-2 Part 1&2. *JAXA research and development report, Japan Aerospace Exploration Agency, Japan.*
- Launder, B.E. and N.D. Sandham (2002). *Closure strategies for turbulent and transitional flows*, Cambridge University Press, Cambridge, UK.
- Scalabrin, L. (2007). Numerical simulation of weakly ionized hypersonic flow over reentry capsules. *PhD. Dissertation, University of Michigan, Michigan.*